DETECTING LOCALIZED VARIATIONS IN THE THREE-DIMENSIONAL FLOW STRUCTURE OF A CONFLUENCE USING THE VELOCITY MAPPING TOOLBOX AND ADCP TECHNOLOGY

An Undergraduate Research Scholars Thesis

by

YAIR TORRES

Submitted to the Undergraduate Research Scholars program at
Texas A&M University
in partial fulfillment of the requirements for the designation as an

UNDERGRADUATE RESEARCH SCHOLAR

Approved by Research Advisor: Dr. Inci Güneralp

May 2019

Major: Environmental Geoscience

TABLE OF CONTENTS

ABSTRACT

Detecting Localized Variations in the Three-Dimensional Flow Structure of a Confluence Using the Velocity Mapping Toolbox and ADCP Technology

Yair Torres
Department of Environmental Programs in Geosciences
Texas A&M University

Research Advisor: Dr. Inci Güneralp
Department of Geography
Texas A&M University

Studies on the complex flow dynamics of fluvial systems have benefited from recent advancements in hydroacoustic technology and post-processing and visualization software. The Velocity Mapping Toolbox (VMT) is one such software that allows users to rapidly process flow-velocity and channel bathymetry data collected along multiple transects into a single-averaged cross section across a river channel. In this study, I aimed to use Acoustic Doppler Current Profiler (ADCP) technology and the VMT, as tools to detect localized variations in three-dimensional flow structure of an asymmetrical river confluence during varying flow conditions. The study site was a reach of the lower Navasota River, which is an anastomosing system located on the border of the Brazos and Grimes counties in Texas. Flow velocity and channel bathymetry data were collected using a Sontek M9 ADCP from January 2019 to March 2019 and processed using the VMT to create three-dimensional flow velocity profiles. Results indicate that only during the highest mean discharge, and when all subchannels were active, was a clockwise helical cell present. During lower flow conditions, a combination of high surface winds, topographic steering, and data quality, lead to difficulties in the interpretation of flow patterns. By further analyzing the complex relationships between three-dimensional flow structure and discharge, this study builds upon the existing knowledge of asymmetrical confluence hydrodynamics and the processing of hydroacoustic river data.

ACKNOWLEDGEMENTS

I would like to thank my advisor, Dr. Inci Güneralp, for her guidance and support throughout the course of this study, and for providing me with the opportunity to conduct high impact learning research.

Additionally, I would like to thank my colleagues in the Fluvial Landscapes and Dynamics Research Group for assisting and guiding me during my research. I would specifically like to thank my graduate-student advisor Cesar Castillo, and FLUD members Andrew Vanderheiden, Dion Webster, Mengqu Han, and Joseph Wade, for assisting me with data collection.

CHAPTER I

INTRODUCTION

The study of rivers is of importance because of their role in the transport of nutrients and sediment, streambank erosion, the surrounding aquatic habitat, and the overall water cycle. River channels are often characterized by their geomorphology and hydraulics (i.e., river flow structure). River geomorphology describes the shape and structure of a river channel and can be studied to understand how the geomorphology affects the distribution of flow within the channel in the downstream, cross-section (transverse), and vertical directions. It also provides insights on how the channel planform has changed and is continuing to change over time. Flow structure on the other hand, is dependent on the river geomorphology, the spatial and temporal variations in discharge, and individual flow velocities. The geomorphology and the flow structure of a river are integral in understanding the current nature of the river and in predicting the future evolution of the river and its aquatic habitat.

Advancements in hydroacoustic technology and post-processing software have facilitated the increased study of fluvial environments and their complex processes. For this reason, the aim of this study is to utilize hydroacoustic surveying and post-processing software to study the complex relationships between three-dimensional flow structure and discharge in an asymmetrical confluence of the Navasota River. The confluence is characterized by the union of a meander bend and two straight subchannels. The Velocity Mapping Toolbox (VMT) (Parsons et al., 2013) will be used to detect the localized variations in flow-velocity profiles during varying hydrological conditions. The information gathered in this study will build upon on

existing knowledge of confluence hydrodynamics and the processing of hydroacoustic-based river-flow and bathymetric data.

Acoustic Doppler Current Profiler

A tool commonly used to study channel geometries and flow structure is an Acoustic Doppler Current Profiler (ADCP). ADCPs work by using the Doppler effect, which centers on the principle that sound waves are at a higher frequency when moving towards you than when moving away. Transducers located on the ADCP instrument emit pulses of sound waves at set frequencies that reflect off particles in the water column and return to the instrument (RD Instruments, 1996). The ADCP can calculate the Doppler shift by tracking the differences between the frequency emitted and the frequencies returned (RD Instruments, 1996). The ADCP pairs the Doppler shift with the time it takes for sound waves to return to the transducer to measure overall flow (RD Instruments, 1996).

Originally, the first generation of ADCPs utilized a narrow-bandwidth and were developed for oceanographic purposes. These first generation ADCPs were first used to measure streamflow data in a riverine environment by Christensen and Herrick (1982) and Simpson and Oltmann (1993). Since then, broadband ADCPs have been developed, which use more of the available bandwidth to capture flow structure data and decrease data variance. This has increased the functionality of ADCPs and allowed them to be used for a multitude of data acquisition purposes in fluvial systems. Early uses of ADCPs found them to be valuable instruments in studying river discharge (Gordon, 1989), suspended sediment loads (Reichel & Natchnebel, 1994), and bed load velocity (Rennie, Millar, & Church, 2002). Furthermore, it was determined that riverine discharge data collected by broadband ADCPs is comparable to stream gauge data (Morlock, 1996). ADCP streamflow measurements were further verified in Oberg and Mueller

(2007). While the above list of uses is not exhaustive, it portrays the flexibility of ADCPs in performing hydroacoustic studies. Due to the increase in ADCP technology and advancements in compatible processing software, ADCPs use has largely replaced traditional streamflow collection methods (Muste, Vermeyen, Hotchkiss & Oberg, 2007).

Acoustic Doppler instruments have been used to measure the three-dimensional flow structure of rivers to better understand the relationship between flow structure and channel planform (Frothingham & Rhoads, 2003; Engel & Rhoads, 2016). In Engel and Rhoads (2016), ADCPs were used to develop contour plots of the two-dimensional and three-dimensional velocities. These contour plots were used to link the patterns of mean flow, bed morphology, and bank erosion. In Frothingham and Rhoads' (2003) acoustic doppler velocimeters were used to measure three-dimensional fluid motion and its influence on the change in channel planform of an asymmetrical meander loop. Three-dimensional flow studies using ADCPs have also been conducted on river confluences with varying configurations. In Rhoads and Johnson (2018), a study was conducted on the three-dimensional flow structure associated with the confluence of a straight tributary and a meander bend. As part of their study, Rhoads and Johnson (2018) emphasized the difficulties associated with definitively characterizing the flows associated with varying confluence configurations. Furthermore, they called for future studies on the three-dimensional structure associated with varying confluences types in order to further understand the complex relationships between river hydrodynamics and channel planform. Thus, a motivating factor for this study

Navasota River – Democrat Crossing

The Navasota River is an anastomosing river that has a length of ~200 kilometers (km), extending from its headwaters in Hill County to its confluence with the Brazos River at the

Brazos-Grimes-Washington County border. Anastomosing rivers can be classified as systems with multiple channels separated by vegetated islands that are relatively stable (Schumm, 1981, 1985). The lower Navasota River is located in the coastal plains of Texas, characterized by a humid subtropical climate. Democrat Crossing in Brazos County is a bridge crossing of Democrat Road over the main channel of the lower Navasota River (Figure 1). The nearest United States Geological Service (USGS) stream gaging station (USGS: 08110800) is ~20 km upstream of Democrat Crossing. Directly upriver of Democrat Crossing, there exists a confluence of the lower Navasota River channel with two of its semi-active subchannels.

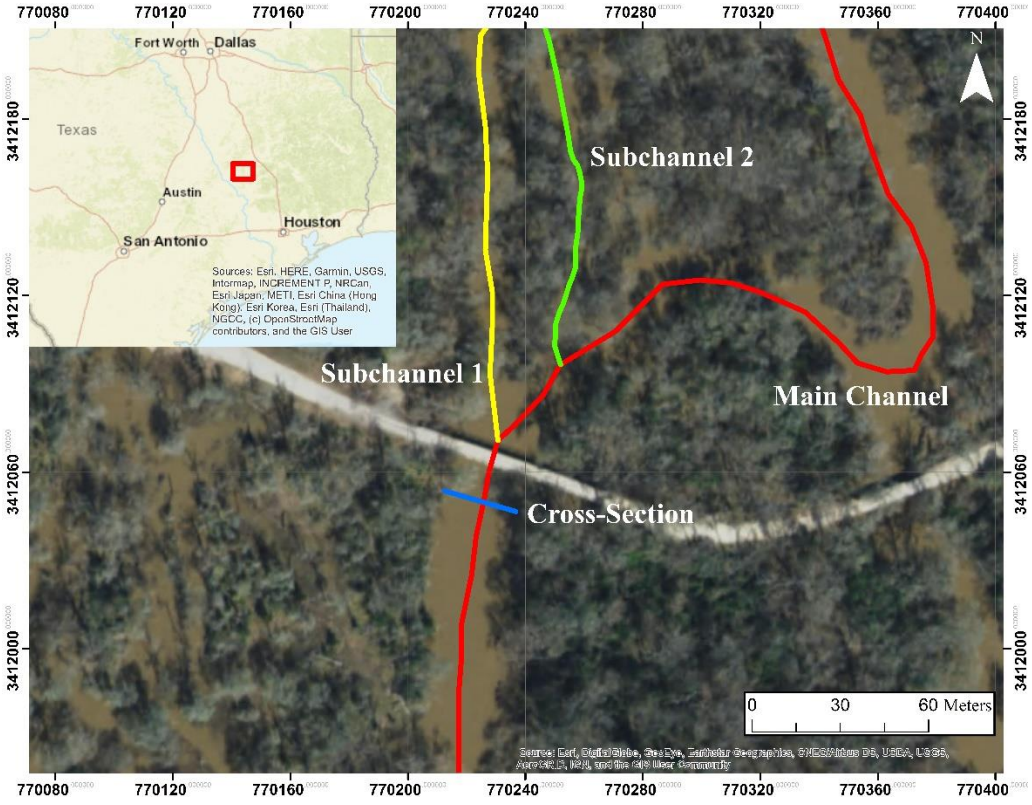

Figure 1. An asymmetrical confluence within the Navasota River. The confluence is characterized by the junction of a meander bend with two straight subchannels. Transects were continuously collected at the same cross-section over three days: January 27th, February 3rd, March 3rd of 2019.

Initial observations of the site indicate complex flows that are governed by the activation of the two subchannels during relatively high flows, as well as backwater effects occurring further upriver at an active meander bend and location of lateral channel migration. These factors result in a highly variable flow structure profile at Democrat Crossing that is dependent on discharge and subchannel activation.

Velocity Mapping Toolbox

The VMT is a post-processing and visualization toolbox developed by the USGS for acoustic surveying data (Parsons et al., 2013) (Figure 2). The toolbox can average bathymetric and flow structure data of multiple cross-section transects into a single representative cross-section (Parsons et al., 2013). It does this by first determining the average cross-section orientation and grid using a least-squares fit. Individual transect data is then projected and interpolated to the cross-section grid using an orthogonal translation. Finally, the arithmetic average of the data at each node on the grid is computed. From these averages, users can visualize a number of flow structure variables and apply the zero-net discharge rotation method or the Rozovskii rotation method (Rozovskii, 1957; Rhoads & Kenworthy, 1998) to the flow data. The Rozovskii method has been found to be especially helpful when attempting to determine the presence of helical motion in strongly converging or diverging flows (Lane, Bradbrook, Richards, Biron, & Roy, 2000)

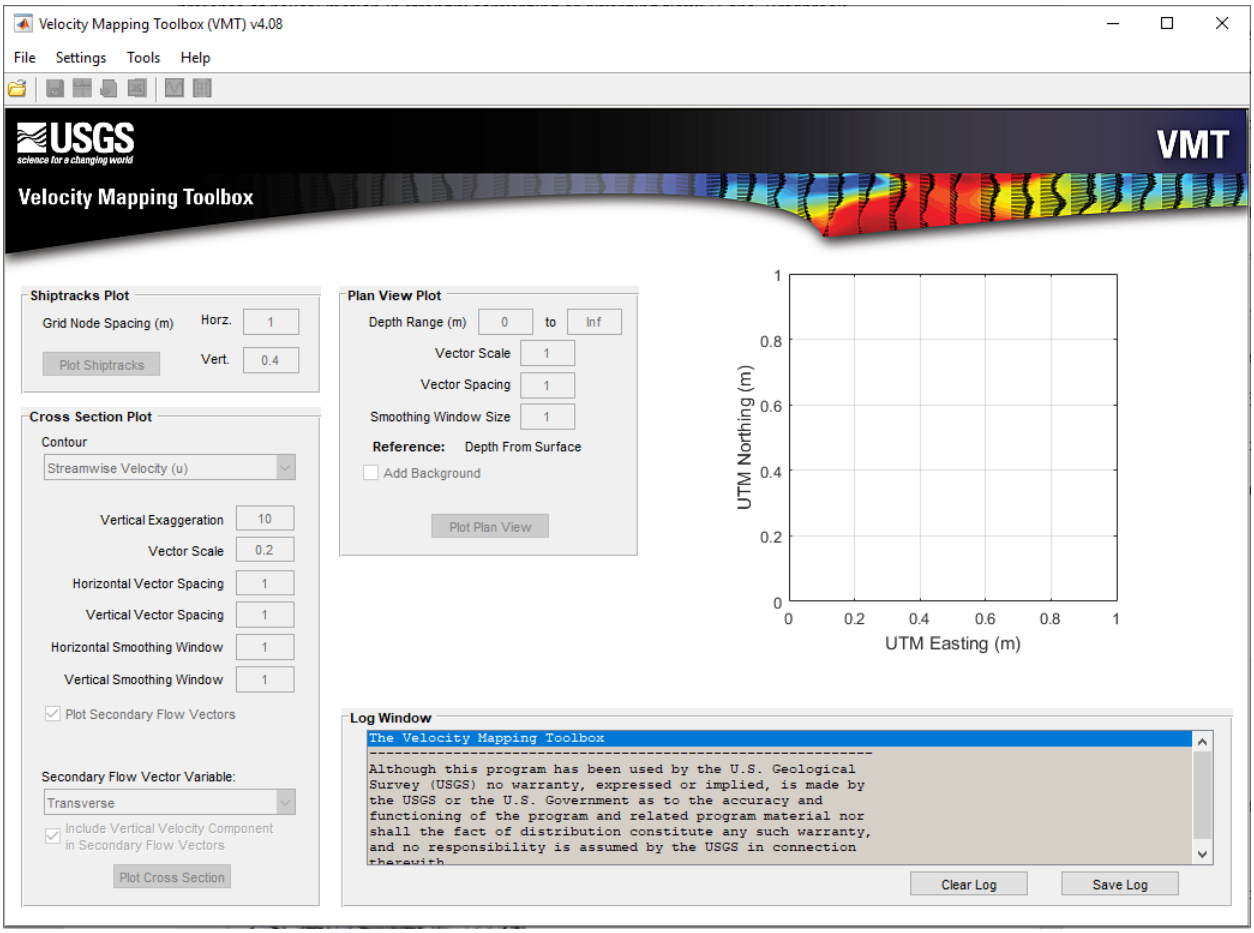

Figure 2. The Velocity Mapping Toolbox user interface.

CHAPTER II

METHODS

Acoustic Doppler Current Profiler Transects

Acoustic surveys were conducted at Democrat Crossing over three days which had separate and varying hydrological conditions: January 27th, February 3rd, and March 3rd of 2019. Three-dimensional flow velocity and bathymetry data were collected using a Sontek M9 ADCP (Figure 3-A). The Sontek M9 utilizes two sets of velocity measurement transducers – four 1-Megahertz (MHz) transducers and four 3-MHz transducers (Sontek, 2017). Additionally, it measures flow depth using a 0.5-MHz vertical beam echo-sounder (Sontek, 2017). Based on the current site conditions, a built-in algorithm, SmartPulseHD, automatically determines the appropriate acoustic pulse scheme at which the transducers emit and collect signals (Sontek, 2017). The Sontek M9 was paired with a Real-Time-Kinematic (RTK) enabled Geographic Positioning System (GPS) to increase the spatial accuracy of the ADCP data. (Figure 3-B). The RTK base station receives GPS data at 10-Hertz (Hz) and transmits RTK corrections to the profiler at 1-Hz. According to the manufacturer, RTK corrections allow for precision to ±3 centimeters (cm) (Sontek, 2017).

The Sontek M9 was mounted on a Sontek Hydroboard floating platform. When securely mounted to the Hydroboard, the bottom of the ADCP sensor extends 7 cm below the surface of the water. To ensure accurate flow structure and discharge measurements, the ADCP's compass was calibrated prior to data collection and the local magnetic declination for the site was manually entered into the ADCP via its companion software, RiverSurveyor Live.

Figure 3. Field Instrumentation. (A) A Sontek M9 ADCP mounted on a Hydroboard was utilized during acoustic surveys. (B) An RTK-GPS Base Station was used to increase the spatial accuracy of ADCP data.

The data collection method involved propelling the Hydroboard manually with ropes by personnel standing on either side of the channel. An attempt was made to maintain the average boat speed equal to or less than the average water speed. Eight transects were collected in reciprocal pairs during each excursion (all at the same cross-section seen on Figure 1), for a total of twenty-four transects. In this case, a transect is defined as traversing the Hydroboard from one bank to the other. Data collected were quality-assured in real-time using RiverSurveyor Live for acceptable boat speed/water speed ratios and variation in total discharge measurements between reciprocal transects.

Velocity Mapping Toolbox Configuration

After being quality-assured, the transects for each of the three days were imported into the VMT as Sontek MAT files. The average cross-section orientations and grids were determined using a horizontal and vertical grid node spacing of 0.25 m and 0.1 m, respectively. After the individual transect data were projected and interpolated onto the cross-section grid, cross-sectional plots were generated. For each day of data collection, a cross-sectional plot was generated to visualize primary flow magnitude and secondary velocity vectors using the

Rozovskii rotation method to better detect the presence of helical motion. A plan view plot of the depth averaged velocity vectors was also generated for each day. A detailed configuration of how both plots were processed and visualized can be found in Table 1 and Table 2. For reference, other configurations of the VMT for data analysis can be found in Parsons et al. (2013). While Parsons et al. (2013) gives detailed explanations and examples of the capabilities of the toolbox, there is no published study which explains in detail the reasoning for certain VMT configurations and what is considered appropriate for each study site. Therefore, informed decisions were made in the configuration of the VMT based on configurations seen in Parsons et al. (2013) and the ADCP data collected. The configuration of the VMT was maintained the same for each data set so that variations in the flow structure produced could not be attributed to different configurations used. For the cross-sectional plots, a horizontal and vertical vector spacing of two was used to acquire an in-ground vector distance of 0.5 m in the horizontal and 0.2 m in the vertical. To spatially average the planform and vector data, a horizontal smoothing window of four and a vertical smoothing window of one was used; creating a smoothing window size of 8x2 per grid node. Further details on how to create and calculate smoothing windows can be found in Parsons et al. (2013).

Table 1. Parameters used in the configuration of the VMT for the generation of cross-sectional plots.

	Cross-Sectional Plot					
Date	**Vert. Exag.**	**Vector Scale**	**Horz. Vector Spacing**	**Vert. Vector Spacing**	**Horz. Smoothing Window**	**Vert. Smoothing Window**
January 27th, 2019	1.5	.04	2	2	4	1
February 3rd, 2019	1.5	.04	2	2	4	1
March 3rd, 2019	1.5	.04	2	2	4	1

Table 2. Parameters used in the configuration of the VMT for the generation of plan view plots.

	Plan View Plot			
Date	**Depth Range (m)**	**Vector Scale**	**Vector Spacing**	**Smoothing Window**
January 27th, 2019	0 to inf.	1	2	4
February 3rd, 2019	0 to inf.	1	2	4
March 3rd, 2019	0 to inf.	1	2	4

Note. Format for Tables 1 and 2 adapted from Parsons et al. (2013). Vert. corresponds with vertical, Exag. with exaggeration, and Horz. with horizontal.

CHAPTER III

RESULTS

Site Conditions

The mean total discharge of transects collected on January 27th was 22.4 cubic meters per second (m^3/s). During these flow conditions, the main channel and both subchannels were inundated and active. The mean total discharge of transects collected on February 3rd and March 3rd was 6.7 m^3/s and 8.9 m^3/s, respectively. During both flow conditions, only the main channel and subchannel 1 were inundated and active. At USGS Gauge: 08110800, there have been 1,008 cases of daily mean discharge above 22.4 m^3/s, 1,571 cases above 8.9 m^3/s, and 1,788 cases above 6.7 m^3/s (Figure 4). Strong surface winds were present on February 3rd and March 3rd, but their magnitudes and directions were not calculated.

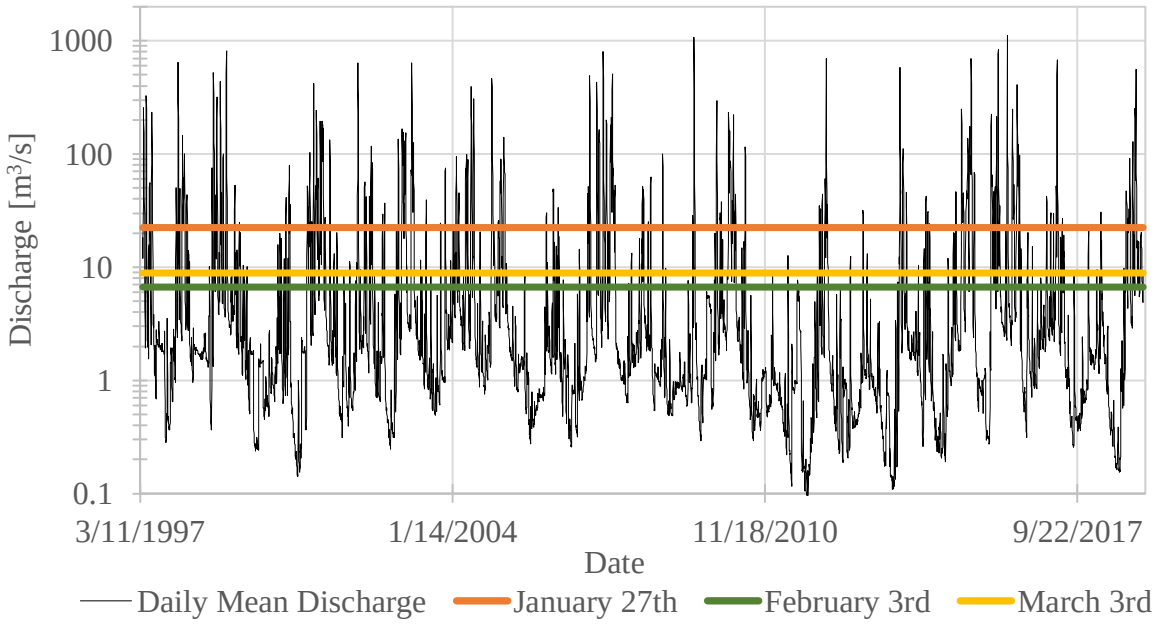

Figure 4. Mean discharge collected by USGS Gauge: 08110800. Mean discharge from 4/1/1997 to 3/3/2019 and the discharge associated with the days when acoustic surveys were conducted.

Flow Structure Profiles

The January 27th plan view plot had relatively small depth averaged velocity (DAV) vectors located near the left bank (Figure 5). These near-bank vectors corresponded with a DAV of 1-20 centimeters per second (cm/s). The largest velocity vectors, DAVs of 40-50 cm/s, were found in the middle of mean transect and over the thalweg, or the deepest part of the channel. Generally, all velocity vectors were faced in a streamwise direction except for the small DAV vectors near the left bank, which faced upstream.

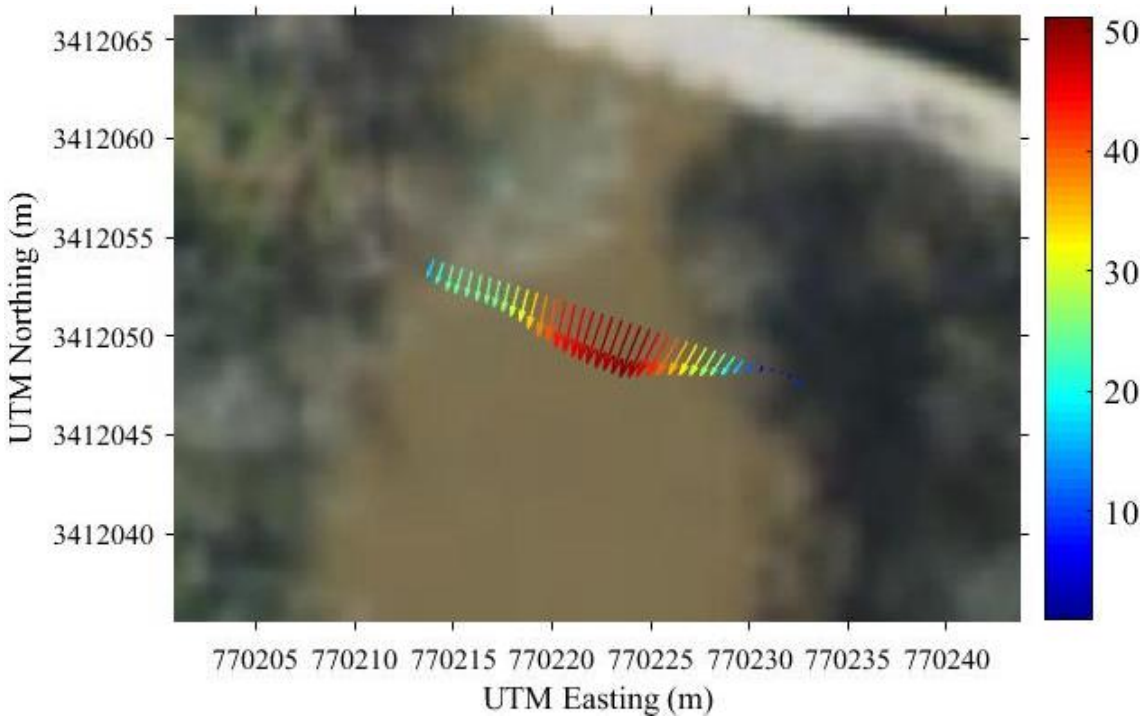

Figure 5. Depth-Averaged-Velocity vectors in cm/s for transects collected on January 27th, 2019.

The plan view plot of flow collected on February 3rd had its smallest velocity vectors located on the left bank, corresponding with a DAV of 1-10 cm/s (Figure 6). The largest velocity vectors were to the right of the thalweg and extended outwards towards the right bank. These vectors had a DAV of 20-30 cm/s. Every vector but two on the left bank, was faced in a streamwise direction. The two vectors on the left bank were faced in an upstream direction.

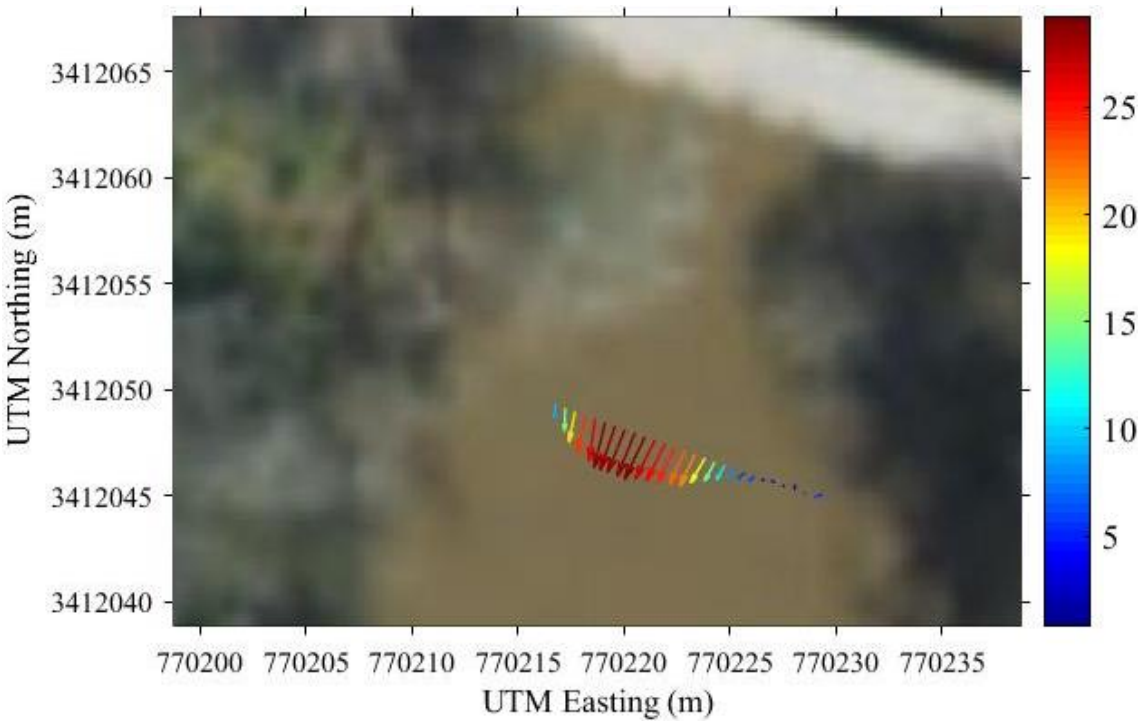

Figure 6. Depth-Averaged-Velocity vectors in cm/s for transects collected on February 3rd, 2019.

The plan view plot for flow collected on March 3rd had its smallest velocity vectors located on the left bank, corresponding with a DAV of 1-10 cm/s (Figure 7). These vectors were faced in an upstream direction. The largest velocity vectors, DAVs of 30-45 cm/s, were found in the middle of the mean transect and slightly to the right of the thalweg. These vectors, while facing in a downstream direction, were slightly skewed towards the center of the high-velocity core.

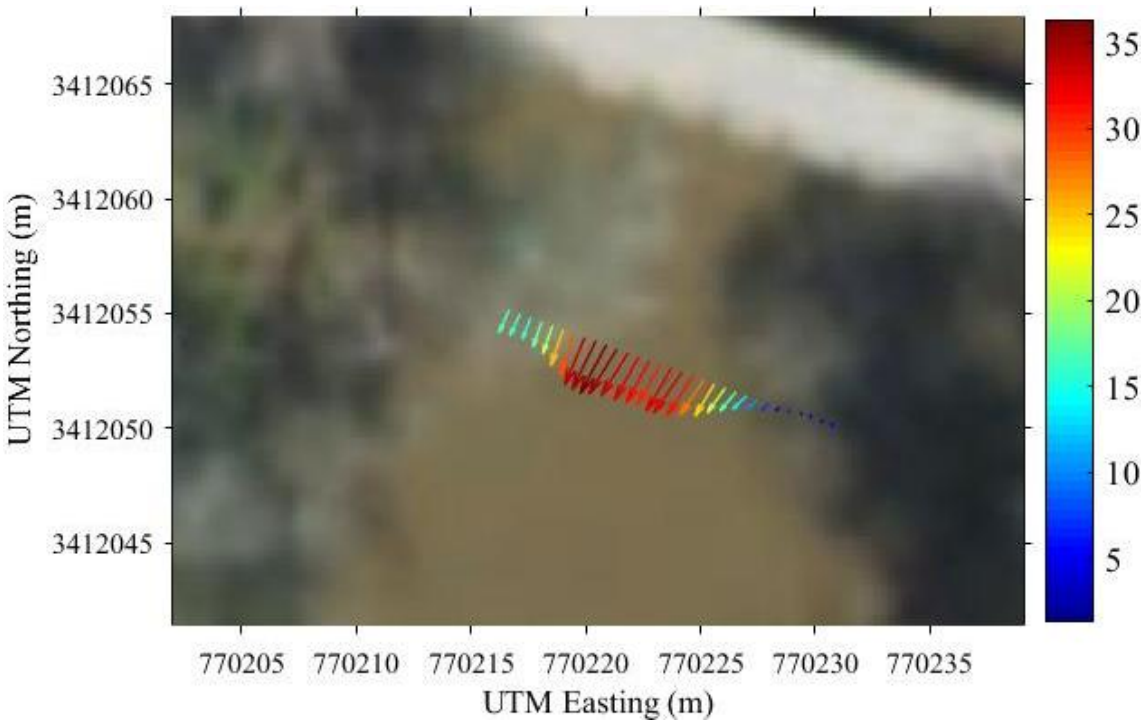

Figure 7. Depth-Averaged-Velocity vectors in cm/s for transects collected on March 3rd, 2019.

The cross-sectional plot for flow collected on January 27th had a centralized and circular high-velocity core over the thalweg, with velocities of 40-60 cm/s (Figure 8). The Rozovskii secondary flow vectors within 6 meters of the left and right banks, pointed both leftwards and rightwards and were of relatively low magnitude at <5 cm/s. Secondary flow vectors within the center of the cross-section and the high-velocity core, depicted movement from the left bank towards the center of the core, before moving downwards and towards the left bank. These flow vectors were of relatively high magnitude, 10-14 cm/s, and increased in magnitude with the clockwise motion. The lowest primary flow magnitude was nearest to the left bank, with flow magnitudes of 0-10 cm/s.

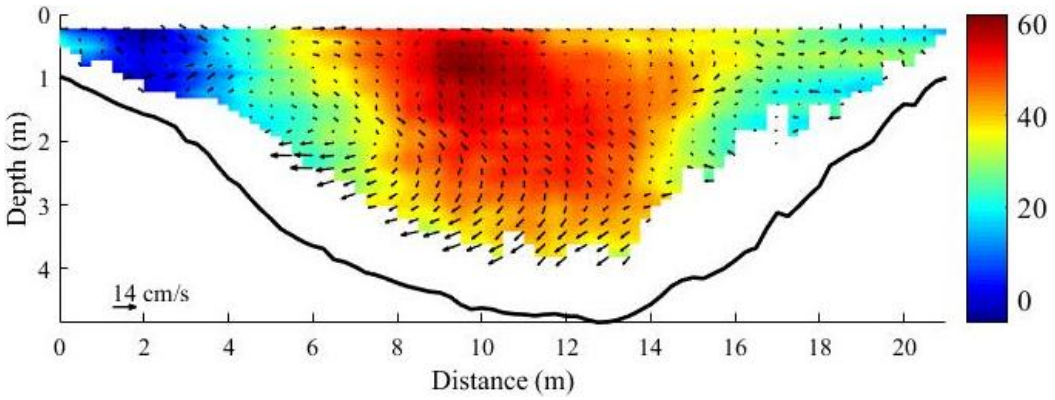

Figure 8. Cross-sectional plot of flow structure on January 27th, 2019. The color map represents the primary flow (looking downstream) in cm/s and the vectors represent the magnitude of the secondary flow in cm/s.

The cross-sectional plot for flow collected on February 3rd had a centralized and ovate high-velocity core with velocities of 20-35 cm/s, extending from the thalweg to the right bank (Figure 9). The Rozovskii secondary flow vectors within two meters of the left and right banks, pointed both leftwards and rightwards. Secondary flow vectors in the top-center of the high-velocity core depicted converging flow patterns. Additionally, secondary flow vectors at the bottom of the high-velocity core and near the channel bed, depicted movement in a clockwise direction. Secondary flow vectors within the entire cross-section were increasingly heterogeneous and varied, regardless of their cross-sectional location, from 2 cm/s to 9 cm/s. The overall lowest primary flow magnitude was nearest to the left bank, with flow magnitudes of -10-0 cm/s.

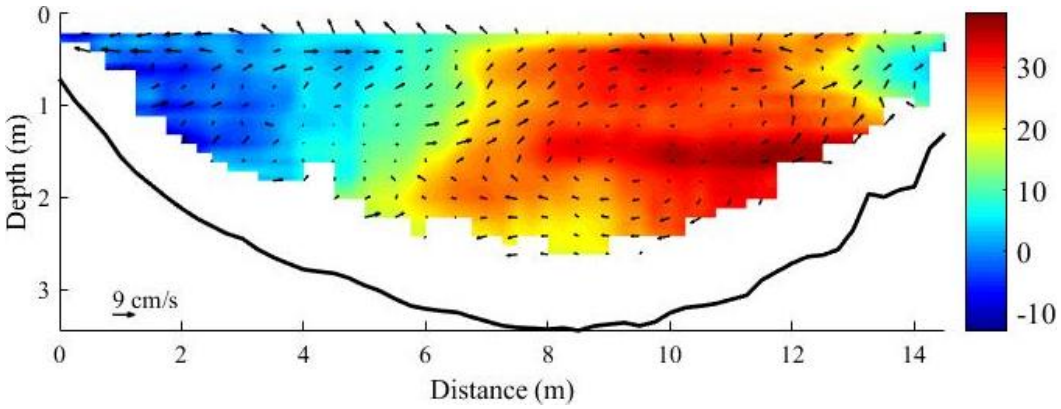

Figure 9. Cross-sectional plot of flow structure on February 3rd, 2019. The color map represents the primary flow (looking downstream) in cm/s and the vectors represent the magnitude of the secondary flow in cm/s.

Similar to the February 3rd cross-section, the cross-sectional plot for flow collected on March 3rd had a centralized and ovate high-velocity core extending from the thalweg to the right bank, but with velocities of 30-45 cm/s (Figure 10).

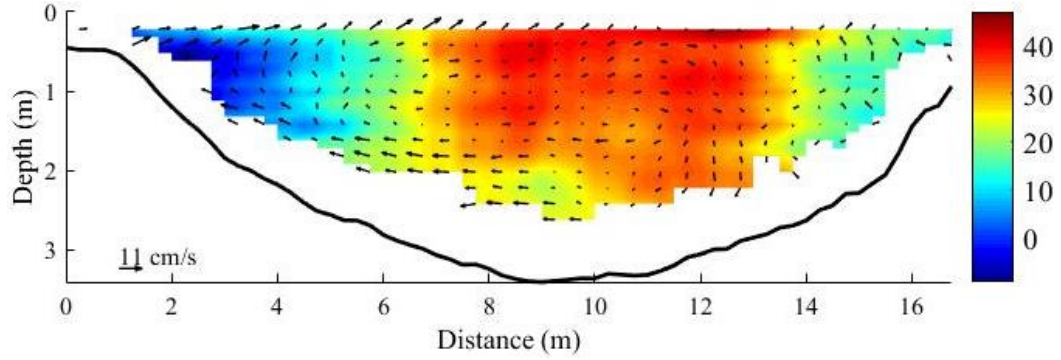

Figure 10. Cross-sectional plot of flow structure on March 3rd, 2019. The color map represents the primary flow (looking downstream) in cm/s and the vectors represent the magnitude of the secondary flow in cm/s.

The Rozovskii secondary flow vectors on the upper portion of the high-velocity core depicted movement from left bank to right bank, and movement from right bank to left bank on the lower portion. Secondary flow vectors within five meters of the left bank, pointed rightwards towards

the center of the channel. As with the February 3rd cross-section, secondary flow vectors within the entire cross-section were increasingly heterogeneous. The flow vectors varied in magnitude, regardless of their cross-sectional location, from 1 cm/s to 14 cm/s.

Cross-sectional data collected for all three days, had the calculated transect discharge vary from 5% to 12%, per reciprocal pairs. The orientation of transects collected on January 27th, February 3rd, and March 3rd deviated from the mean streamwise direction by an average of 2.3 degrees, 11.5 degrees, and 8.9 degrees, respectively. All within the acceptable 20 degrees in deviation for when calculating secondary flow (Bever & MacWilliams, 2016).

CHAPTER IV

DISCUSSION

Velocity Vector Profiles

Patterns of the DAV vectors and the location of the high-velocity cores from all three flows show that as discharge increases in the channel, the stream-wise velocity profile shifts towards the left bank, indicating a dominance in flow from the main channel and subchannel 2. This is likely due to the orientation of the confluence, permitting the union of the main channel with subchannel 2, prior to their union with subchannel 1.

In the January 27th cross-sectional plot, Rozovskii secondary flow vectors depicted movement from the left bank towards the center of the cross-section, before moving downwards and towards the left bank again. This can be classified as helical motion due to the convergence of channel flows. The flow patterns of the secondary vectors seen in the February 3rd cross-section, depict not only converging flows near the surface, but to some degree the presence of helical motion. The converging vectors could be attributed to the presence of support pillars directly upstream from the cross-section. Flow bifurcates around the pillars and converges again downstream. This convergence of flows would explain the secondary flow vector patterns. The March 3rd cross-sectional plot had secondary flow vectors with increasingly heterogenous flow patterns. The vectors not only varied in magnitude but also in direction. While some patterns exist between the top and bottom of the cross-section, none that can be definitively attributed to confluence dynamics or helical cells.

All three plan view plots had small DAV vectors on the left bank which were faced in an upstream direction. When compared to the cross-sectional plots, this area of backwater effect

coincides with the location of reduced primary flow magnitudes. These flow patterns are likely due to the presence of downed wood on the left bank. While the extent of the influence is not quantified here, it is evident that the downed wood has a hydrodynamic impact on the flow structure of the confluence.

Data Quality Control

In some cases, reciprocal transects varied by more than 5% in total mean discharge recorded, which could have had an impact on the flow profiles produced. Furthermore, the site of the cross-section for this study is downstream of a bridge supported by columns that extend into the channel. The support columns undoubtedly disrupt the confluence flow structure and likely had an influence the data collected by the ADCP. It's important to also note the presence of high surface winds during acoustic surveys conducted on February 3rd and March 3rd. These surface-winds along with downed wood, would have impacted the flow structure data collected by the ADCP. In terms of data-processing, the VMT had a high sensitivity to user defined configurations, which led to variations in the 3D flow velocities produced, depending on the configuration selected. The VMT recommended grid node sizes of ~2 cm for the three data sets, which is not appropriate for the acoustic data collected. This points to a potential error in the data collection process, or defects in the ADCP used.

CHAPTER V

CONCLUSION

Studies on the relationship between flow structure and channel geomorphology in river systems have greatly benefited from recent advancements in hydroacoustic technology. Concurrently, the development of post-processing and visualization products such as the VMT, have increased large data management and analyses capabilities. In this study, ADCP technology and the VMT were used as tools to detect and analyze the localized variations in three-dimensional flow structure during varying hydrological conditions in an asymmetrical confluence. It was determined that only during relatively higher mean discharges (>22 m^3/s), where all three channels were inundated and active, was a clockwise helical cell present. During lower flow conditions, a combination of high surface winds, topographic steering, and data quality issues, lead to difficulties in the interpretation of flow patterns.

Moving forward, more transects should be conducted at different cross-sections throughout the confluence and into the individual channels in order to have a more definitive understanding of the hydrodynamics associated with this system. The data collected should be tied to channel activation, the associated momentum flux, discharge ratios, and stream power. Furthermore, in order to build on the existing framework of post-processing acoustic survey data in the VMT, detailed VMT configurations and their explanations are required. Issues with the quality of the data could have played a factor in the interpretations of the three-dimensional flow profiles. In conclusion, by further analyzing the complex three-dimensional flow structure associated with an asymmetrical confluence with semi-active channels, this study helps build on

existing knowledge of confluence hydrodynamics and the VMT processing of hydroacoustic-based river-flow and bathymetric data.

REFERENCES

Bever, A. J., & MacWilliams, M. L. (2016). Factors influencing the calculation of periodic secondary circulation in a tidal river: numerical modelling of the lower Sacramento River, USA: Periodic Secondary Circulation in a Tidal River. *Hydrological Processes*, *30*(7), 995–1016.

Christensen, J. L., & Herrick, L. E. (1982). *Mississippi River test, v. 1., Final Rep. DCP4400/300, prepared for the U.S. Geological Survey: AMETEK/Straza Division*. El Cajon, CA: U.S. Geological Survey.

Engel, F. L., & Rhoads, B. L. (2016). Three-dimensional flow structure and patterns of bed shear stress in an evolving compound meander bend. *Earth Surface Processes and Landforms*, *41*(9), 1211–1226.

Frothingham, K. M., & Rhoads, B. L. (2003). Three-dimensional flow structure and channel change in an asymmetrical compound meander loop, Embarras River, Illinois. *Earth Surface Processes and Landforms*, *28*(6), 625–644.

Gordon, R. L. (1989). Acoustic Measurement of River Discharge. Journal of Hydraulic Engineering, 115(7), 925–936.

Lane, S. N., Bradbrook, K. F., Richards, K. S., Biron, P. M., & Roy, A. G. (2000). Secondary circulation cells in river channel confluences: measurement artefacts or coherent flow structures? *Hydrological Processes*, *14*(11–12), 2047–2071.

Morlock, S. (1996). *Evaluation of Acoustic Doppler Current Profiler measurements of river discharge*. Water-Resources Investigations Report 95-4218. Reston, VA: U.S. Geological Survey.

Muste, M., Vermeyen, T., Hotchkiss, R., & Oberg, K. (2007). Acoustic Velocimetry for Riverine Environments. *Journal of Hydraulic Engineering*, *133*(12), 1297–1298.

Oberg, K., & Mueller, D. S. (2007). Validation of Streamflow Measurements Made with Acoustic Doppler Current Profilers. *Journal of Hydraulic Engineering*, 133(12), 1421–1432.

Parsons, D. R., Jackson, P. R., Czuba, J. A., Engel, F. L., Rhoads, B. L., Oberg, K. A., … Riley, J. D. (2013). Velocity Mapping Toolbox (VMT): a processing and visualization suite for moving-vessel ADCP measurements. *Earth Surface Processes and Landforms*, *38*(11), 1244–1260.

RD Instruments. (1996). *Acoustic Doppler Current Profiler Principles of Operations: A Practical Primer*. San Diego, CA: RD Instruments.

Reichel, G., & Natchnebel, H. P. (1994). Suspended sediment monitoring in a fluvial environment: Advantages and limitations applying an Acoustic Doppler Current Profiler. Water Research, 28(4), 751–761.

Rennie, C. D., Millar, R. G., & Church, M. A. (2002). Measurement of Bed Load Velocity using an Acoustic Doppler Current Profiler. *Journal of Hydraulic Engineering*, *128*(5), 473–483.

Rhoads, B. L., & Johnson, K. K. (2018). Three-dimensional flow structure, morphodynamics, suspended sediment, and thermal mixing at an asymmetrical river confluence of a straight tributary and curving main channel. *Geomorphology*, *323*, 51–69.

Rhoads, B. L., & Kenworthy, S. T. (1998). Time-averaged flow structure in the central region of a stream confluence. *Earth Surface Processes and Landforms*, *23*(2), 171–191.

Rozovskii, I. L. (1957). Flow of Water in Bends of Open Channels. Academy of Sciences of the Ukrainian SSR, Kiev.

Schumm, S. A. (1981). Evolution and response of the fluvial system, sedimentologic implications. *Society of Economic Paleontologist and Mineralogist Special Publication*, 31, 19-29.

Schumm, S. A. (1985). Patterns of Alluvial Rivers. *Annual Review of Earth and Planetary Sciences*, *13*(1), 5–27.

Simpson, M. R., and Oltmann, R. N. (1993). *Discharge-measurement system using an acoustic Doppler current profiler with applications to large rivers and estuaries*. Water-Supply Paper 2395. Reston, VA: U.S. Geological Survey.

Sontek. (2017). *RiverSurveyor S5/M9 System Manual Firmware Version 4.02*(Rep.). San Diego, CA: Xylem.